

Tidal Effects and the Proximity Decay of Nuclei

A. B. McIntosh, S. Hudan, C. J. Metelko, and R. T. de Souza

Department of Chemistry and Indiana University Cyclotron Facility, Indiana University, Bloomington, Indiana 47405, USA

R. J. Charity and L. G. Sobotka

Department of Chemistry, Washington University, St. Louis, Missouri 63130, USA

W. G. Lynch and M. B. Tsang

National Superconducting Cyclotron Laboratory and Department of Physics and Astronomy, Michigan State University, East Lansing, Michigan 48824, USA

(Received 10 August 2006; revised manuscript received 30 March 2007; published 27 September 2007)

We examine the decay of the 3.03 MeV state of ^8Be evaporated from an excited projectilelike fragment following a peripheral heavy-ion collision. The relative energy of the daughter α particles exhibits a dependence on the decay angle of the $^8\text{Be}^*$, indicative of a tidal effect. A comparison of the measured tidal effect with a model suggests a measurable nuclear proximity interaction.

DOI: [10.1103/PhysRevLett.99.132701](https://doi.org/10.1103/PhysRevLett.99.132701)

PACS numbers: 25.70.Ef, 21.10.Tg, 25.70.Mn

Aggregation of clusters in a dilute medium is a process that impacts a wide range of physical phenomena from the formation of galactic structure to the formation of van der Waals clusters in a low density gas. Examples of such aggregation which involve the delicate interplay of elementary forces are the formation of pasta nuclei in a neutron star crust [1,2] or alpha clustering in both low density nuclear matter [3] and light nuclei [4]. For heavy nuclei, cluster aggregation is manifested by emission of clusters, from the common process of α decay to emission of more exotic clusters such as ^{14}C [5]. The reduced density near the nuclear surface allows formation of clusters and their emission. Cluster emission thus primarily probes the surface properties of the emitting nucleus [6]. Our present understanding of cluster emission is largely based upon the yields, kinetic energy spectra, and angular distributions of emitted clusters—all well described within a statistical transition-state formalism [7]. In this Letter we present clear evidence for the interaction of the emitted cluster with the nuclear surface. Using resonance spectroscopy we explore how the $^8\text{Be}^*$ decay is impacted by the tidal effect [8]. Modification of resonance peak masses and widths in relativistic heavy-ion collisions has been used to provide insight on the interaction of the medium at hadronic freeze-out with the resonant species [9].

Charged particles from the reaction $^{114}\text{Cd} + ^{92}\text{Mo}$ at $E/A = 50$ MeV were detected in a 4π setup. We selected peripheral collisions through detection of projectilelike fragments (PLFs) with $10 \leq Z \leq 48$ with a segmented annular Si(IP)/CsI(Tl) telescope, in the angular range $2.1^\circ \leq \theta^{\text{lab}} \leq 4.2^\circ$ with $\Delta\theta^{\text{lab}} \approx 0.13^\circ$ [10]. This PLF is the decay residue of the excited primary projectilelike fragment (PLF*) formed by the collision. Charged particles with $Z \leq 9$ were isotopically identified in the angular range $7^\circ \leq \theta^{\text{lab}} \leq 58^\circ$ with the silicon-strip array LASSA [11,12]. Each LASSA telescope consisted of a

stack of two $5 \text{ cm} \times 5 \text{ cm}$ silicon-strip detectors [Si(IP)] backed by a 2×2 arrangement of CsI(Tl) crystals each with photodiode readout. Each telescope, segmented into 16×16 orthogonal strips, had good angular resolution ($\Delta\theta^{\text{lab}} \approx 0.43^\circ$). The LASSA array was centered at $\theta^{\text{lab}} = 32^\circ$ with respect to the beam axis. The identification threshold of LASSA is 2 MeV/A for α particles. For the following analysis, events were selected with $15 \leq Z_{\text{PLF}} \leq 46$, $V_{\text{PLF}} \geq 8.0$ cm/ns and the multiplicity of particles in LASSA, $N_{\text{LASSA}} = 2, 3$. Using the measured emitted particles and the assumption of isotropy, the Z , A , and velocity of the PLF* were calculated [13]. For these events, the most probable atomic number of the PLF* is ≈ 30 .

The kinetic energy spectra of ^4He and Be nuclei emitted in the angular range $\theta_{\text{PLF}^*} \leq 80^\circ$ are presented in Fig. 1. These spectra are reasonably described by a Maxwell-

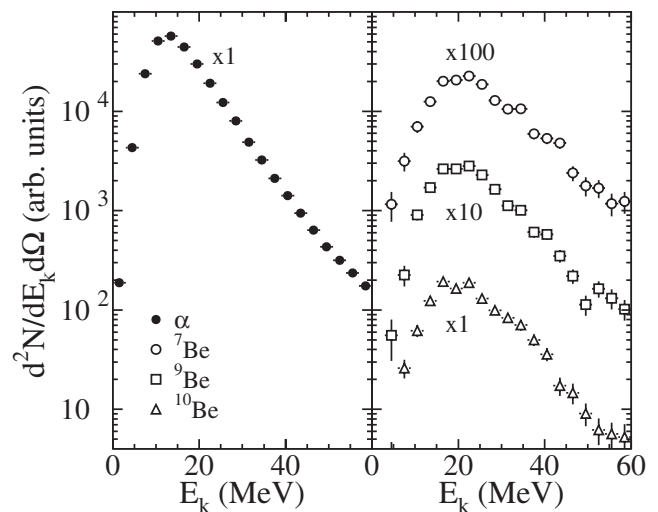


FIG. 1. Kinetic energy spectra of α particles and $^{7,9,10}\text{Be}$ fragments in the PLF* frame observed with $\theta_{\text{PLF}^*} \leq 80^\circ$.

Boltzmann distribution consistent with evaporation [13]. The larger average kinetic energy of ${}^7\text{Be}$, as compared to that of ${}^{9,10}\text{Be}$, has been interpreted as the sequential decay of excited primary fragments as they propagate away from the emitting nucleus [10]. For the events presented, the PLF* has a most probable excitation energy of 3 MeV/A and a maximum excitation of 4 MeV/A, consistent with the “temperature” associated with the α particle kinetic energy spectra [13]. The impact of secondary decay on the trend extracted in the subsequent analysis was calculated to be insignificant.

The decay of short-lived resonant states such as ${}^8\text{Be}^*$ emitted in the deexcitation cascade of the PLF* can be examined by constructing the relative energy spectrum of the daughter products. Shown in Fig. 2(a) is the relative energy spectrum of two α particles for events in which either two or three α particles were detected in LASSA with $\theta_{\alpha, \text{PLF}^*} \leq 100^\circ$. Solid symbols depict the experimental data which exhibits a peak at ≈ 3 MeV. The overall shape of the spectrum is affected at low $E_{\text{rel}} (\leq 2 \text{ MeV})$ by the finite angular acceptance of the LASSA CsI(Tl) detectors, as two particles entering the same CsI(Tl) crystal are not resolved. Thus, the ${}^8\text{Be}$ ground state is not observed in this kinematic regime. For larger $E_{\text{rel}} (\geq 5 \text{ MeV})$, the yield is impacted by the geometric acceptance of LASSA. The relative energy distribution has two primary components: resonant decay of ${}^8\text{Be}^*$ and nonresonant α emission. To assess the nonresonant contribution, a “background” for the resonant decay, we performed a mixed-event analysis. Two α particles were selected from different events and their relative energy was calculated. The number of mixed

events calculated was 20 times the coincident yield; hence, its statistical contribution to the subsequent error analysis is negligible. The resulting spectrum, shown in Fig. 2(a) (open squares), was normalized in the interval $14 \leq E_{\text{rel}} \leq 50 \text{ MeV}$. While the mixed-event background has the general shape of the observed relative energy spectrum, there is an excess yield in the observed data centered at $\approx 3 \text{ MeV}$ due to the decay of the first excited state of ${}^8\text{Be}$ at 3.03 MeV. The mixed-event spectrum has a larger yield for $E_{\text{rel}} \leq 1.5 \text{ MeV}$ as mixed pairs do not experience Coulomb repulsion. As events sampled in the mixed-event analysis span an artificially broad distribution of PLF* velocities, we restricted the difference in PLF* velocity, ΔV_{PLF^*} , between two events. The mixed-event background corresponding to $\Delta V_{\text{PLF}^*} \leq 0.6 \text{ cm/ns}$, which provides a good description for $6 \leq E_{\text{rel}} \leq 50 \text{ MeV}$, is shown in Fig. 2(a) (open triangles). This background also provides a better description of the data for $E_{\text{rel}} \leq 1.5 \text{ MeV}$ while it exhibits a larger yield at $E_{\text{rel}} \approx 3 \text{ MeV}$.

To better understand the background, we have modeled the nonresonant final-state interaction with a Monte Carlo Coulomb trajectory calculation. In this model (MC-FSI), two α particles are isotropically emitted from the nuclear surface in sequential fashion. The $(Z, A, V, \text{ and } \theta)_{\text{PLF}^*}$ are taken from the experimental data while the time between emissions is taken to be exponential with a mean time τ . Following Coulomb propagation, all particles were filtered for the experimental acceptance, angular resolution, and thresholds. Calculations with $\tau = 100, 300, \text{ and } 500 \text{ fm/c}$ are shown in Fig. 2(b) along with the experimental data and mixed-event background. With decreasing mean emission time, suppression of yield for low values of E_{rel} is observed. While the calculation with $\tau = 100 \text{ fm/c}$ is inconsistent with the experimental data, $\tau \geq 300 \text{ fm/c}$ provides a reasonable description of the mixed-event background for $E_{\text{rel}} \geq 2 \text{ MeV}$. A deduced mean emission time of this magnitude for $E^* \approx 3 \text{ MeV/A}$ is consistent with previous work [14]. Comparing the mixed-event background with the MC-FSI results reveals that for all but the smallest values of E_{rel} the mixed-event background provides a reasonable description of the nonresonant contribution.

The first excited state of ${}^8\text{Be}$ has an intrinsic width of 1.5 MeV [15], corresponding to a mean lifetime of $\approx 131 \text{ fm/c}$. For such a short lifetime, the likelihood that this state decays in the vicinity of the emitting nucleus is significant. Consequently, as the ${}^8\text{Be}^*$ decays into two α particles, its increasing quadrupole moment interacts with the gradient of the Coulomb field of the emitting nucleus. For α pairs which decay orthogonal to the emission direction, the field gradient acts to increase their relative energy. In contrast, α pairs which decay along the emission direction experience a reduced relative energy due to the larger acceleration of the nearer α particle [8]. In order to examine this Coulomb tidal effect, we constructed the difference relative energy spectra of the observed α pairs and the

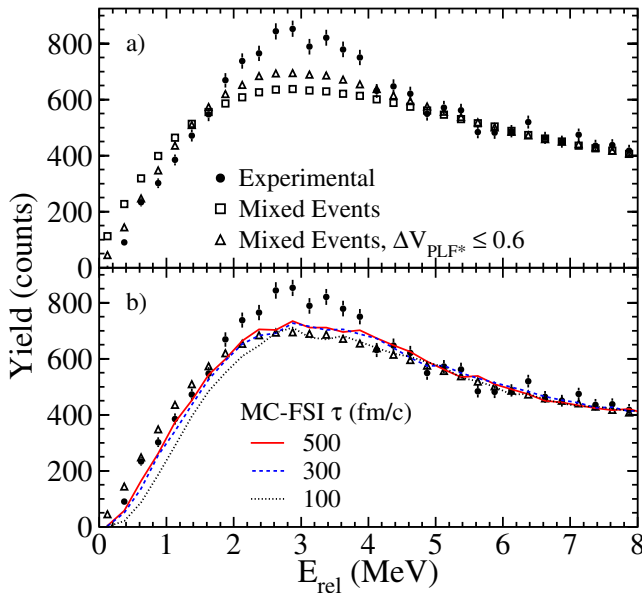


FIG. 2 (color online). Panel (a): Relative kinetic energy distributions for α - α pairs. Panel (b): Comparison of the mixed events with Monte Carlo calculations of a nonresonant final-state interaction.

mixed-event background. These spectra were constructed for different decay angles, β , calculated as the angle between the relative momentum and the center-of-mass momentum of the α - α pair. Depicted in Fig. 3 is the case using the mixed-event background with $\Delta V_{\text{PLF}^*} \leq 0.6$ cm/ns (solid symbols) and with no restriction on ΔV_{PLF^*} (open symbols). The ΔV_{PLF^*} restriction does not introduce a major change in the difference relative energy spectra. The prominent feature of the difference spectra evident for all β is the peak at ≈ 3 MeV. It is evident that the peak in the difference spectrum for $0 \leq \beta \leq 45^\circ$ is shifted to lower values of E_{rel} as compared to larger values of β . To quantitatively extract the dependence of $\langle E_{\text{rel}} \rangle$ on β for the 3.03 MeV state, we integrated the difference spectra in the region indicated by the vertical lines. These integration limits were selected by considering the shape of the experimental distributions and the results of Monte Carlo simulations for the emission and decay of ${}^8\text{Be}^*$. These simulations, described below, describe the resonant decay of the ${}^8\text{Be}^*$ accounting for the intrinsic width of the 3.03 MeV state, the tidal effect, and the detector acceptance. In fact, the extracted $\langle E_{\text{rel}} \rangle$ is relatively insensitive to any reasonable choice of integration limits.

The dependence of the average relative energy, $\langle E_{\text{rel}} \rangle$, on the decay angle β is shown in Fig. 4 as solid symbols. A clear manifestation of a tidal effect is observed as $\langle E_{\text{rel}} \rangle$ increases with increasing β . The magnitude of the ob-

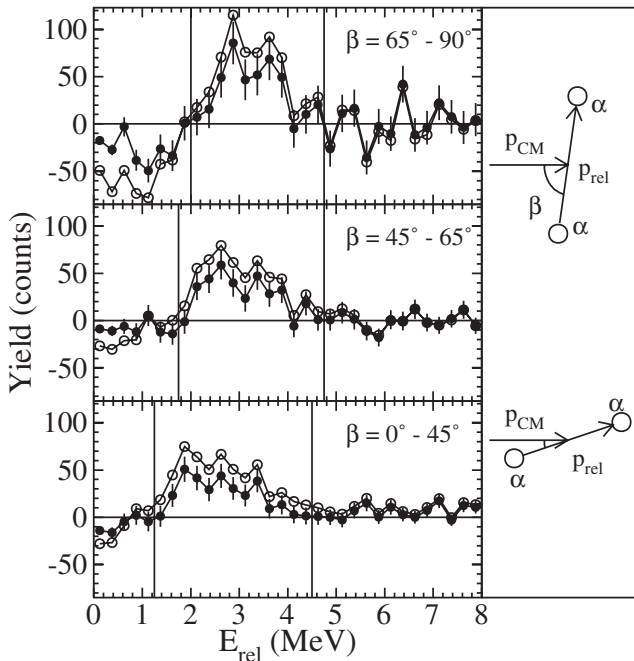


FIG. 3. Difference relative energy spectra of observed α pairs for different decay angles, β , relative to the mixed-event background. Solid symbols reflect a mixed-event background with $\Delta V_{\text{PLF}^*} \leq 0.6$ cm/ns; open symbols correspond to no ΔV_{PLF^*} restriction. Error bars show statistical uncertainties.

served change in $\langle E_{\text{rel}} \rangle$ is ≈ 0.65 MeV, a relative change of $\approx 20\%$. The error bars shown, while dominated by the measurement statistics, include the uncertainty associated with the integration limits. To demonstrate the sensitivity of $\langle E_{\text{rel}} \rangle$ to different mixed-event backgrounds we also show as open symbols the dependence of $\langle E_{\text{rel}} \rangle$ on β for no restriction on ΔV_{PLF^*} . The same overall trend of $\langle E_{\text{rel}} \rangle$ on β is observed for the different mixed-event conditions.

To understand this observation quantitatively, we simulated the decay of a ${}^8\text{Be}^*$ in a Monte Carlo model, MC-Res. In this model the ${}^8\text{Be}^*$ is emitted from the surface of the PLF^* . The position vector is chosen to be isotropic while the initial velocity is radially oriented. The properties of the PLF^* were sampled as in the MC-FSI calculations. Reflecting first order kinetics, the lifetime of the emitted ${}^8\text{Be}^*$ was chosen with a probability distribution $P(t) = \exp(-t/\tau)$ with the mean lifetime, τ , taken as 131 fm/c given by the intrinsic state width. The initial kinetic energy of the ${}^8\text{Be}^*$ is taken to be exponential with a slope parameter of 7.5 MeV, indicative of thermal emission and consistent with the experimental data shown in Fig. 1. The ${}^8\text{Be}^*$ propagates in the Coulomb field of the PLF^* residue as a point particle until it decays. At the moment of decay the ${}^8\text{Be}^*$ is replaced with two α particles with an inter- α separation (scission configuration) given by $R_{\alpha-\alpha} = 5.81$ fm in accordance with systematics [16]. A smaller $R_{\alpha-\alpha}$ of 4 fm makes a negligible difference in the results. The decay angle, β , of the two α system with respect to the emission direction is taken to be isotropic; i.e., we neglect the effect the field has in orienting the ${}^8\text{Be}^*$. Following decay, the two α particles are propagated along trajectories determined by the three-body Coulomb interaction. Energy

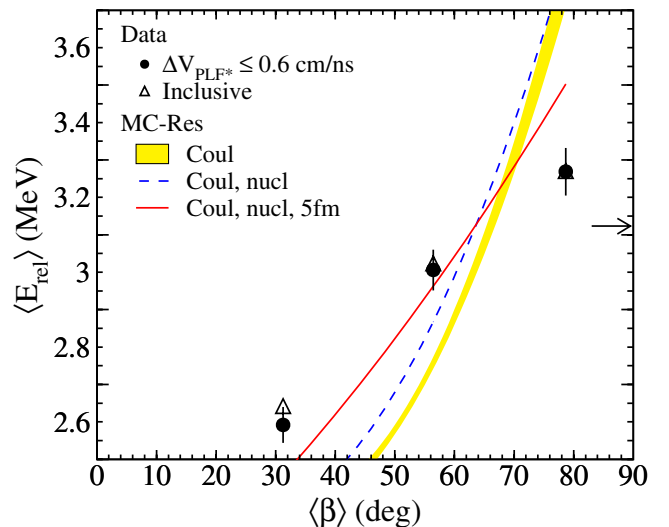


FIG. 4 (color online). Dependence of $\langle E_{\text{rel}} \rangle$, of two α particles from the decay of ${}^8\text{Be}(3.03 \text{ MeV})$, on the average decay angle, $\langle \beta \rangle$. Lines represent the results of Monte Carlo calculations for resonance decay. The arrow corresponds to the sum of the intrinsic energy of the state and the decay Q value.

and momentum are conserved at all stages of the calculation. Particles are subsequently filtered by the detector acceptance, angular resolution, and thresholds.

We have also investigated the impact of deformation of the $\text{PLF}_{\text{res}}^*$ [17] and thermal fluctuations of its radius on the predicted tidal effect. To simulate the deformation of the $\text{PLF}_{\text{res}}^*$ in the direction of the separation axis with the targetlike fragment following the collision we replaced the spherical $\text{PLF}_{\text{res}}^*$ with a dinuclear configuration (touching spheres) of a ^{12}C nucleus and the corresponding residue, with emission of the $^8\text{Be}^*$ from the residue. This dinuclear configuration of the $\text{PLF}_{\text{res}}^*$ is a reasonable approximation of the average configuration experienced by the earliest $^8\text{Be}^*$ emissions. To probe the influence of thermal fluctuations which alter the initial $\text{PLF}_{\text{res}}^* - ^8\text{Be}^*$ separation, we varied the $\text{PLF}_{\text{res}}^*$ radius assuming the magnitude of the fluctuations had a standard deviation of 1 fm. The results of these Coulomb calculations are represented by the shaded band in Fig. 4. The dependence of $\langle E_{\text{rel}} \rangle$ on β is clearly overestimated by this Coulomb calculation. Even with these uncertainties this Coulomb model cannot explain the weaker tidal effect measured in the experimental data.

To examine the influence of the nuclear potential which is particularly important for short-lived decays we replaced the Coulomb potential in the previous simulation with a potential that includes both nuclear and Coulomb parts: $V_{\text{tot}} = \frac{1.44Z_1Z_2}{r} + \frac{U_s}{1 + \exp(\frac{r-R_s}{a_s})}$ where $U_s = -100$ MeV and the diffuseness $a_s = 0.8$ fm. The value of R_s is chosen so that for different $\text{PLF}_{\text{res}}^*$ sizes the “top of the barrier” is consistent with systematics [16]. The initial position of the $^8\text{Be}^*$ is taken as the top of the barrier with an initial kinetic energy consistent with an exponential energy spectrum with $T = 7.5$ MeV. The result of this calculation is indicated by the dashed (blue) line in Fig. 4. Clearly the gradient of the potential alone is incapable of explaining the magnitude of the measured tidal effect.

One possible reason the dependence of $\langle E_{\text{rel}} \rangle$ on β is weaker in the experimental data as compared to the nuclear calculation is the interaction of the emitted $^8\text{Be}^*$ with the nuclear surface. This interaction is particularly important as the most probable initial velocity of the $^8\text{Be}^*$ is close to zero and it consequently spends a significant time within the range of the proximity interaction. This is in contrast to the tidal decay following projectile breakup reactions [18]. An attractive surface interaction can stabilize the $^8\text{Be}^*$ while it is in the vicinity of the emitting nucleus resulting in a decreased dependence of $\langle E_{\text{rel}} \rangle$ on β . Such a stabilization would be analogous to the binding of the halo neutrons in ^{11}Li . Systematic changes in the width of the 2^+ state of ^8Be have previously been observed in direct reactions and attributed to the interaction with the spectator particle [19]. To simulate the impact of such a stabilization on the tidal effect, we prevented the $^8\text{Be}^*$ from decaying when its center-of-mass was within a certain “stabilization distance” of the top of the barrier. The result

of a calculation with a stabilization distance of 5 fm is shown as the solid (red) line in Fig. 4. While the predicted dependence of $\langle E_{\text{rel}} \rangle$ on β is reduced, the magnitude of the measured trend is still not reproduced within this schematic model.

In summary, we have measured the dependence of $\langle E_{\text{rel}} \rangle$ on decay angle for the first excited state of ^8Be . Qualitatively, a dependence of $\langle E_{\text{rel}} \rangle$ on decay angle can be understood as a tidal effect in which the decaying cluster interacts with the gradient of an external field provided by the emitting nucleus. Calculations with a simple Coulomb model over predict the observed dependence. Inclusion of a nuclear potential reveals that the gradient alone is insufficient to explain the quantitative dependence of the measured $\langle E_{\text{rel}} \rangle$ on decay angle. Interactions of the decaying cluster with the nuclear surface, which may act to stabilize the excited cluster due to the attractive nuclear potential, could play a role in explaining the magnitude of the observed trend. A more detailed investigation of the interplay between Coulomb and nuclear effects that impact the proximity decay of the short-lived cluster could provide new information about the characteristics of nascent clusters.

We would like to acknowledge the valuable assistance of the staff at MSU-NSCL for providing the high quality beams which made this experiment possible. This work was supported by the U.S. Department of Energy under No. DE-FG02-88ER-40404 (IU), and No. DE-FG02-87ER-40316 (WU) and the National Science Foundation under Grant No. PHY-95-28844 (MSU).

-
- [1] D. G. Ravenhall *et al.*, Phys. Rev. Lett. **50**, 2066 (1983).
 - [2] C. J. Horowitz *et al.*, Phys. Rev. C **69**, 045804 (2004).
 - [3] G. Röpke *et al.*, Phys. Rev. Lett. **80**, 3177 (1998).
 - [4] A. Tohsaki *et al.*, Phys. Rev. Lett. **87**, 192501 (2001).
 - [5] H. J. Rose and G. A. Jones, Nature (London) **307**, 245 (1984).
 - [6] L. G. Sobotka and R. J. Charity, Phys. Rev. C **73**, 014609 (2006).
 - [7] L. G. Moretto, Nucl. Phys. **A247**, 211 (1975).
 - [8] R. J. Charity *et al.*, Phys. Rev. C **63**, 024611 (2001).
 - [9] P. F. Kolb and M. Prakash, Phys. Rev. C **67**, 044902 (2003).
 - [10] S. Hudan *et al.*, Phys. Rev. C **71**, 054604 (2005).
 - [11] B. Davin *et al.*, Nucl. Instrum. Methods Phys. Res., Sect. A **473**, 302 (2001).
 - [12] A. Wagner *et al.*, Nucl. Instrum. Methods Phys. Res., Sect. A **456**, 290 (2001).
 - [13] R. Yanez *et al.*, Phys. Rev. C **68**, 011602(R) (2003).
 - [14] L. Beaulieu *et al.*, Phys. Rev. Lett. **84**, 5971 (2000).
 - [15] D. R. Tilley *et al.*, Nucl. Phys. **A745**, 155 (2004).
 - [16] L. G. Sobotka *et al.*, Phys. Rev. Lett. **51**, 2187 (1983).
 - [17] S. Hudan *et al.*, Phys. Rev. C **70**, 031601(R) (2004).
 - [18] R. J. Charity *et al.*, Phys. Rev. C **52**, 3126 (1995).
 - [19] E. H. Berkowitz, Nucl. Phys. **60**, 555 (1964).